RSC Advances

ROYAL SOCIETY OF CHEMISTRY

www.rsc.org/advances

RSC Advances

ARTICLE

A carbon fiber based three-phase heterostructures composite CF/$Co_{0.2}Fe_{2.8}O_4$/PANI as an efficient electromagnetic wave absorber in K_u band

Received 00th January 20xx,
Accepted 00th January 20xx

DOI: 10.1039/x0xx00000x

www.rsc.org/

Jiyong Fang, Zheng Chen, Wei Wei, Yunxi Li, Tao Liu, Zhi Liu, Xigui Yue*, and Zhenhua Jiang

A three-phase heterostructures composite CF/$Co_{0.2}Fe_{2.8}O_4$/PANI with a layer by layer (LBL) structure was designed and synthesized for achieving improvement on electromagnetic (EM) wave attenuation of carbon fiber (CF). The structure and morphology analyses demonstrated the LBL structure of the absorber. The electromagnetic parameters of absorber and wax composite were measured at 2-18 GHz to evaluate its EM wave attenuation performance. The three-phase heterostructures absorber CF/$Co_{0.2}Fe_{2.8}O_4$/PANI demonstrated the highest attenuation effectiveness value of -38.2 dB (> 99.9 % attenuation) at 12.7 GHz with a thickness of 4.1 mm. Moreover, for CF/$Co_{0.2}Fe_{2.8}O_4$/PANI, with an absorber thickness of 3.1-4.1 mm, the minimum RL values are all lower than -20 dB in K_u band. The excellent EM wave absorbency in K_u band for CF/$Co_{0.2}Fe_{2.8}O_4$/PANI results from the combined effect of magnetic loss and dielectric loss by introducing more phase onto CF. Considering the EM wave absorption performance and the effortless fabrication process, it is believable that by introducing more specially designed phase, the EM wave attenuation performance of CF can be significantly improved.

Introduction

In recent years, with the rapid development of the electronics industry, electromagnetic (EM) wave pollution has already been a crucial global issue, as it can interfere with the surrounding electronic devices, and harm human health.[1] Hence, it is of great importance to shield and absorb both the incoming and outgoing EM wave radiation around us. Additionally, in military field, it is well known that the stealth performance of the weapons and equipment (aircrafts, ships, tanks) can greatly improve their strike capability and viability in the battlefield.[2] Therefore, for the big demand in civil and military fields, EM wave absorption and shielding materials have already attracted a great deal of attention from all over the world and have already been widely investigated in both academic and industrial labs. As a result, several kinds of materials have already been found to possess the EM wave absorption properties, for instance, magnetic particles (Fe_3O_4, Co_3O_4, $CoFe_2O_4$, carbonyl iron, Fe_2O_3), [3-9] ferrite ($BaFe_{12}O_{19}$, $BaCo_2Fe_{16}O_{27}$), [10] nanoparticles (Ag, Ni, Fe, Co, ZnO, CeO_2), [11-14] conductive polymers (PANI, PPy), [15-17] carbon materials (CNTs, graphene, graphite, carbon black, amorphous carbon, carbon fiber), [1, 12, 18-23] metallic perovskite lanthanum nickel oxide, [24] and magnetic-dielectric hybrids. [25, 26] Among those materials, carbon based EM wave absorbers have attracted considerable attention from all over the world for their excellent mechanical, electrical, and thermal properties together with their low density property. [27] For these reasons, carbon fibers (CF), as an excellent carbon material, have great potential in future EM absorption field, not only because of their lightweight, large aspect ratio, high strength and good conductivity, but also for their thermal and chemical stabilities, and low manufacturing cost.

However, for unilateral dielectric loss materials or magnetic loss materials, it is hard to attain a desired impedance matching condition. According to the transmission line theory, it is obvious that the EM wave absorption performance is mainly determined by the electromagnetic properties of the synthesized material, that is, the relative complex permittivity ($\varepsilon_r = \varepsilon' - j\varepsilon''$) and the relative complex magnetic permeability ($\mu_r = \mu' - j\mu''$). For a better EM absorption behavior, the balance between the permittivity and the magnetic permeability (EM impedance matching) is critical. Consequently, in order to improve the EM wave absorbency, it is an effective way to combine the dielectric loss components with the magnetic loss particles to achieve a desirable impedance matching situation. [28, 29] Thus, it is believable that the EM wave absorbency of CF can be improved through chemical modification. Great efforts have already been taken to improve the EM wave absorption behavior of carbon fiber. CF/carbonyl iron core-shell structure composites have been prepared by Liu and coworkers with a method of metal organic chemical vapor deposition. [30] And

Alan G. MacDiarmid Institute, College of Chemistry, Jilin University, 2699 Qianjin street, Changchun 130012, People's Republic of China
Email: yuexigui@jlu.edu.cn; Tel:+86-431-85168868
Electronic Supplementary Information (ESI) available: SEM image of the received chopped carbon fiber, SEM of the cross section view for CF/$Co_{0.2}Fe_{2.8}O_4$/PANI, the relationship between RL and EM wave frequency of CF/$Co_{0.2}Fe_{2.8}O_4$, coefficient matching factor of the absorbers and the loss tangent and EM wave spread schemes of CF/$Co_{0.2}Fe_{2.8}O_4$. See DOI: 10.1039/x0xx00000x

Shen et al reported that Ferrite and short carbon fiber composites can be used to improve the EM wave absorbency of CF. [10] Many other works have been done to further improve the EM wave attenuation performance of CF. [31-33] However, few absorbers have been reported to exhibit a reflection loss that exceeds -30 dB (Table 1). As a consequence, it is of profound importance to design other CF based absorbers using some feasible methods to achieve improvement on the EM wave absorption performance.

Hence, in this study, a three-phase heterostructures absorber CF/$Co_{0.2}Fe_{2.8}O_4$/PANI with a layer by layer (LBL) structure was specially designed to improve the EM wave absorption performance of CF. In our work, CF was firstly coated with a layer of magnetic nanoparticles ($Co_{0.2}Fe_{2.8}O_4$) to optimize the EM parameters for a fine impedance matching. Moreover, outside the magnetic particles layer, a layer of conductive polymer (polyaniline, PANI) was further used, not only to further enhance the EM wave absorption properties, but also to improve the dispersion characteristics when used in polymer matrix. By introducing more interface, the three-phase heterostructure absorber was expected to own an excellent EM wave attenuation ability. The structure, morphology, complex permittivity and permeability, and EM wave absorption of the absorber are investigated in detail.

Experimental

Materials

Chopped carbon fiber (CF, average diameter 14.5 μm, average length 0.15 mm) was supplied by Kureha. $FeCl_2$ •$4H_2O$ (Alfa Aesar), $CoCl_2$ •$6H_2O$ (Aladdin Chemistry Co.Ltd) and $FeCl_3$ •$6H_2O$ (Sigma-Aldrich) were all used as received. Aniline was purchased from Sinopharm Chemical Reagent and purified by distillation under reduced pressure before used. All the other chemicals obtained from reagent suppliers (Beijing Chemical Works, or Tianjin Chemical Reagent) were used without further purification unless otherwise noted.

Synthesis of CF/$Co_{0.2}Fe_{2.8}O_4$ two-phase heterostructures

The synthesis of CF/$Co_{0.2}Fe_{2.8}O_4$ two-phase heterostructures was carried out in a 500 ml three necked flask. In a typical experiment, with the protection of nitrogen, distilled water (300 ml), CF (0.7 g), $FeCl_3$ •$6H_2O$ (7.35 mmol, 1.9867 g), $FeCl_2$ •$4H_2O$ (2.94 mmol, 0.5845 g), and $CoCl_2$ •$6H_2O$ (0.74 mmol, 0.1749 g) were added. The mixture was rapidly heated to 70°C with a mechanical stirring (800 rpm). Subsequently, some NH_3 •H_2O was added to the above mixture to make pH=10. After being heated at 70°C for 1 hour, the products were collected by centrifugation and washed thoroughly by deionized water and ethanol to remove impurities.

Synthesis of CF/$Co_{0.2}Fe_{2.8}O_4$/PANI three-phase heterostructures

For the fabrication of CF/$Co_{0.2}Fe_{2.8}O_4$/PANI three-phase heterostructures, to a suspension of the as prepared CF/$Co_{0.2}Fe_{2.8}O_4$ (0.7 g in 170 ml distilled water), phosphoric acid (85 wt%, 0.56 ml) and aniline (1.12 ml) were added. After being cooled to 0 °C by an ice bath with stirring, 100 ml ammonium persulfate (APS) aqueous solution (25.76 mg/ml) was dropwise added into the above dispersion in one hour. The suspension was stirred at 0°C for 24 hours. After that, the precipitations were collected by centrifugation. Finally, the products were washed with distilled water and ethanol for several times, followed by drying in a vacuum oven at 60°C.

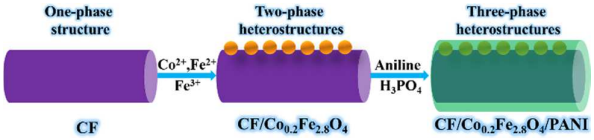

Scheme 1. The synthesis route of CF/$Co_{0.2}Fe_{2.8}O_4$/PANI

Measurement

Fourier transform infrared (FT-IR) spectroscopy was carried out on a Nicolet Impact 410 Fourier transform infrared (FT-IR) spectrometer with a mixture of KBr (nonabsorbent medium) and sample (weight ratio sample/KBr=1:100). X-ray powder diffraction (XRD) was performed on a PANalytical B.V. Empyrean system (Cu Kα) in the scattering range of 10°-80°. The magnetic properties of the synthesized materials were measured by a vibrating sample magnetometer (VSM) (SQUID-VSM, America, 298 K). Scanning electron microscopy (SEM) images were obtained on a FEI Nova Nano 450 field emission SEM system and samples were platinum coated. An Oxford X-Max energy dispersion X-ray spectrometry (EDX) system was applied to determine the elemental analysis information. The thermal property of the synthesized materials was detected by thermogravimetric analysis (TGA) (PerkinElmer TGA-7, heating rate of 20 °C min^{-1} and under an N_2 flow rate of 50 ml min^{-1}). The relative permeability and permittivity was obtained on an Agilent N5244A PNA-X network analyzer in the frequency range of 2–18 GHz for the calculation of reflection loss (RL) by the coaxial reflection/transmission method based on NRW method. The sample containing composite materials and paraffin wax with the mass ratio of 1:2 was pressed into toroidal-shaped samples (ϕout=7.00 mm, ϕin=3.04 mm, thickness=2 mm) for microwave measurement. The simulated reflection loss (RL) was calculated from the measured parameters according to the transmission line theory.

Results and discussion

Structural analysis

As shown in Scheme 1, a CF based three-phase layer by layer heterostructures absorber was specially designed and synthesized for the improvement in the EM wave absorption performance of CF. $Co_{0.2}Fe_{2.8}O_4$ nanoparticle with a higher magnetization saturation (M_s) and better EM wave absorption property, as reported in the previous work of our lab, was selected to optimize the EM parameters for a fine impedance matching. [34] And PANI was further used to enhance the EM wave absorbency. To investigate the structural information of the synthesized materials, XRD pattern and FT-IR spectroscopy were applied.

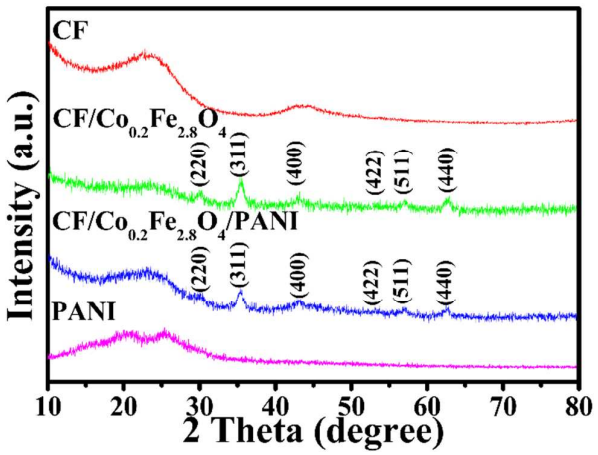

Fig. 1. The XRD patterns of CF, PANI, CF/$Co_{0.2}Fe_{2.8}O_4$, CF/$Co_{0.2}Fe_{2.8}O_4$/PANI.

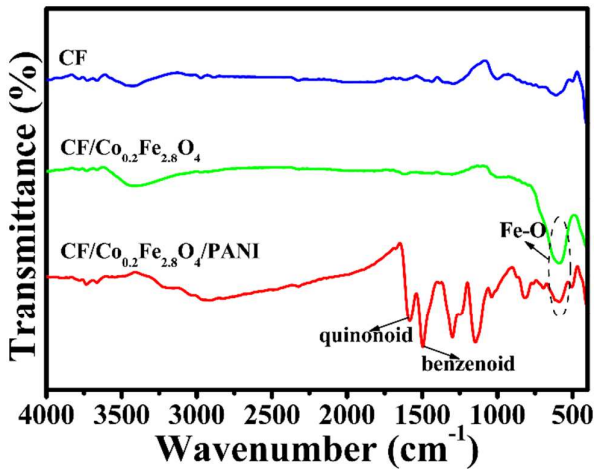

Fig. 2. The IR spectra of CF, CF/$Co_{0.2}Fe_{2.8}O_4$, CF/$Co_{0.2}Fe_{2.8}O_4$/PANI.

Figure 1 shows the XRD patterns of CF and the synthesized materials. CF exhibits two peaks at 23.5°and 44.1°, which can be indexed to the (002) and (100) crystal plane of hexagonal graphite. [12] However, the peaks are broad, indicated the relatively low crystallinity degree and the amorphous nature of CF. Compared to the XRD pattern of CF, six more peaks appear in the XRD pattern of CF/$Co_{0.2}Fe_{2.8}O_4$, which are belong to $Co_{0.2}Fe_{2.8}O_4$. The series of diffraction peaks at 2θ = 30.2°, 35.5°, 43.2°, 53.6°, 57.3°and 63.0°are assigned to the (220), (311), (400), (422), (511) and (440) planes of the face centred cubic lattice of $Co_{0.2}Fe_{2.8}O_4$, respectively. [35, 36] According to Debye-Scherrer equation (D=Kλ/Bcosθ), the $Co_{0.2}Fe_{2.8}O_4$ particles are about 10.8 nm. [34] The absence of impurity peaks in the XRD pattern indicates that the synthesized $Co_{0.2}Fe_{2.8}O_4$ nanoparticles have a high degree of purity. The result shows that CF was coated with a layer of magnetic nanoparticles ($Co_{0.2}Fe_{2.8}O_4$). For CF/$Co_{0.2}Fe_{2.8}O_4$/PANI, it is hard to observe obvious diffraction peaks that belongs to PANI, because the diffraction peaks of PANI and CF are almost centered at the same 2θ. However, it is worthwhile to note that the diffraction peaks of CF/$Co_{0.2}Fe_{2.8}O_4$/PANI are consistent with CF/$Co_{0.2}Fe_{2.8}O_4$, suggesting the presence of $Co_{0.2}Fe_{2.8}O_4$ nanoparticles in the three-phase heterostructures composite after coating with a layer of PANI. Thus, FT-IR was used to detect the PANI layer.

To further verify the structure of the obtained absorber CF/$Co_{0.2}Fe_{2.8}O_4$/PANI, FT-IR spectroscopy is applied as shown in Fig. 2. The spectra of pure CF and CF/$Co_{0.2}Fe_{2.8}O_4$ are also shown for comparison. In contrast to the spectrum of CF, strong absorption peak at 584 cm^{-1} (Fe-O stretching vibration) appears in that of CF/$Co_{0.2}Fe_{2.8}O_4$ and CF/$Co_{0.2}Fe_{2.8}O_4$/PANI, which is an obvious evidence of the $Co_{0.2}Fe_{2.8}O_4$ layer on CF. [37] According to the result of CF/$Co_{0.2}Fe_{2.8}O_4$/PANI, when coated with a layer of PANI, there are more peaks which are signals of the PANI layer. In the spectrum of CF/$Co_{0.2}Fe_{2.8}O_4$/PANI, the peaks at 1581 and 1490 cm^{-1} are assigned to the stretching deformations of C=N bond in quinoid ring and C=C bond in benzenoid ring in PANI units, respectively. And the peaks at 1297 and 1240 cm^{-1} in the three-phase heterostructures are due to the C–N stretching of secondary aromatic amine, while the peak around 1142 cm^{-1} is attributed to the aromatic C–H in-plane bending for benzenoid ring in PANI. [15,17] The above FT-IR results indicate the successful coating process of PANI layer. From the XRD and FT-IR results, it is apparent that $Co_{0.2}Fe_{2.8}O_4$ nanoparticles and PANI were successfully synthesized on the surface of CF. However, the LBL structure of CF/$Co_{0.2}Fe_{2.8}O_4$/PANI still remain invisible.

Morphological analysis

In order to determine the LBL structure of CF/$Co_{0.2}Fe_{2.8}O_4$/PANI and the situation of $Co_{0.2}Fe_{2.8}O_4$ nanoparticles and PANI supported on

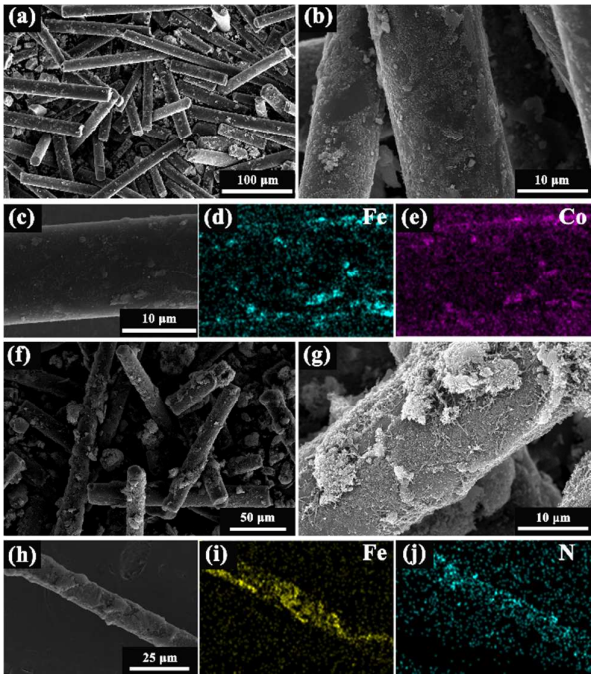

Fig. 3. (a-c)The SEM images of CF/$Co_{0.2}Fe_{2.8}O_4$; (d and e) the EDX elemental mapping information of CF/$Co_{0.2}Fe_{2.8}O_4$; (f-h) the SEM images of CF/$Co_{0.2}Fe_{2.8}O_4$/PANI; (i and j) the EDX elemental mapping information of CF/$Co_{0.2}Fe_{2.8}O_4$/PANI.

the surface of CF, both SEM and EDX elemental mapping techniques were all taken to examine the structure and morphology of the products. The results are presented in Fig. 3. Clearly, as shown in Fig. 3a and 3b, the CF/$Co_{0.2}Fe_{2.8}O_4$ composite has rough surfaces, compared to that of CF (Fig. S1), indicating that CF was successfully coated with a layer of $Co_{0.2}Fe_{2.8}O_4$ nanoparticles. Shown in Fig. 3f and 3g are the typical morphology of the synthesized three-phase heterostructures absorber CF/$Co_{0.2}Fe_{2.8}O_4$/PANI. When coated with PANI, the surface of CF/$Co_{0.2}Fe_{2.8}O_4$ became rougher, demonstrating the existence of PANI coating layer. Moreover, larger average diameter was observed in the synthesized CF/$Co_{0.2}Fe_{2.8}O_4$/PANI compared to that of CF/$Co_{0.2}Fe_{2.8}O_4$, because of the outside PANI polymer layer. Also SEM images of the cross section for CF/$Co_{0.2}Fe_{2.8}O_4$/PANI was provided in Fig. S2. From the SEM results, obviously, the three-phase heterostructures CF/$Co_{0.2}Fe_{2.8}O_4$/PANI with a LBL structure was successfully prepared. Supporting the SEM results, EDX elemental mapping data can be a cogent evidence. Fig. 3d-e show the corresponding EDX elemental mapping of Fe (Kα) and Co (Kα) for CF/$Co_{0.2}Fe_{2.8}O_4$. It is clear that the elements Fe (Fig. 3d) and Co (Fig. 3e) are evenly distributed throughout the whole surface of CF based on the SEM image in Fig.3c, which suggests that the $Co_{0.2}Fe_{2.8}O_4$ nanoparticles covered on CF and formed two-phase heterostructures. When CF/$Co_{0.2}Fe_{2.8}O_4$ was coated with PANI, shown in Fig. 3i-j, the elements Fe (Kα, Fig. 3i) and N (Kα, Fig. 3j) were detected. Element N which belongs to PANI, is uniform dispersed in the heterostructures referred to SEM image shown in Fig.3h. The EDX elemental mapping result is accordant with the above SEM data, indicating the LBL structure characteristic of CF/$Co_{0.2}Fe_{2.8}O_4$/PANI. However, the content of each layer remain to be further investigated. The particular layer LBL structure will endow CF/$Co_{0.2}Fe_{2.8}O_4$/PANI with some exceptional properties, for instance, magnetic property, permittivity and permeability, which can finally influence its EM wave absorbency.

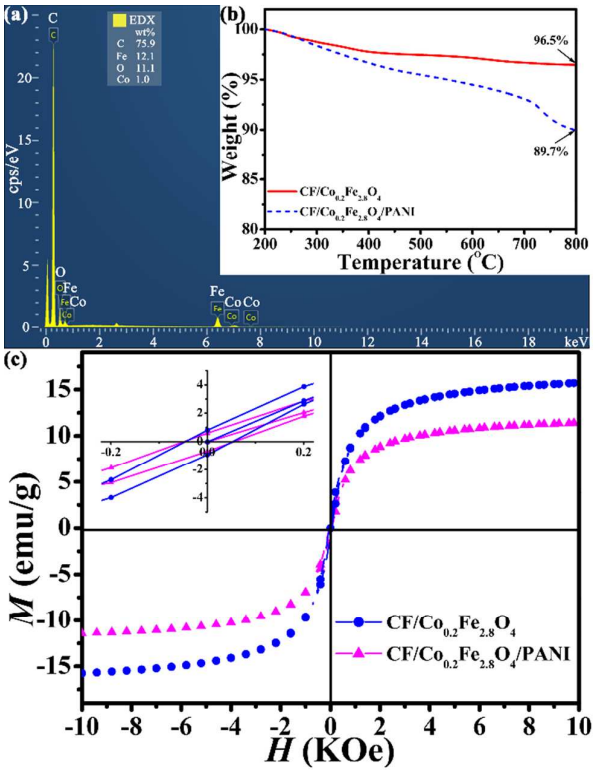

Fig. 4. (a) EDX elemental data of CF/$Co_{0.2}Fe_{2.8}O_4$; (b) TGA curves of CF/$Co_{0.2}Fe_{2.8}O_4$ and CF/$Co_{0.2}Fe_{2.8}O_4$/PANI; (c) *M-H* loops of CF/$Co_{0.2}Fe_{2.8}O_4$ and CF/$Co_{0.2}Fe_{2.8}O_4$/PANI, and the insert is the enlarge of *M-H* loops of CF/$Co_{0.2}Fe_{2.8}O_4$ and CF/$Co_{0.2}Fe_{2.8}O_4$/PANI.

Composition analysis and magnetic property

In this work, $Co_{0.2}Fe_{2.8}O_4$ and PANI were particularly chosen as the coating layer on CF to obtain a desired EM wave absorption performance. The content of each layer in CF/$Co_{0.2}Fe_{2.8}O_4$/PANI was investigated by EDX and TGA data in Fig. 4a and 4b. From the EDX elemental information, it is obvious that the weight ratio of $Co_{0.2}Fe_{2.8}O_4$ is about 24.1% in CF/$Co_{0.2}Fe_{2.8}O_4$. Based on the obtained TGA data of CF/$Co_{0.2}Fe_{2.8}O_4$ and CF/$Co_{0.2}Fe_{2.8}O_4$/PANI at 800°C, the content of PANI is about 7.0% in CF/$Co_{0.2}Fe_{2.8}O_4$/PANI according to the equation ((1-wt%$_{PANI}$)×0.965=0.897). As a consequence, in the three-phase LBL heterostructure absorber CF/$Co_{0.2}Fe_{2.8}O_4$/PANI, the content of CF, $Co_{0.2}Fe_{2.8}O_4$ and PANI are about 70.6%, 22.4% and 7.0%, respectively. In the specially designed three-phase LBL structure absorber, $Co_{0.2}Fe_{2.8}O_4$ nanoparticles performed as a promoter to increase the complex permeability of the microwave absorber to achieve a fine matching condition. Considering the relatively low content of the magnetic component, *M-H* loops in Fig. 4c demonstrate that both CF/$Co_{0.2}Fe_{2.8}O_4$ and CF/$Co_{0.2}Fe_{2.8}O_4$/PANI maintain good superparamagnetic property of the $Co_{0.2}Fe_{2.8}O_4$ nanoparticles with the M_s reached to 16 and 12 emu g^{-1}, respectively. It is believable the magnetic property may contribute to the complex permeability of CF/$Co_{0.2}Fe_{2.8}O_4$/PANI to achieve a better matching condition between the complex permittivity and permeability.

Permittivity and permeability

The microwave absorbency of an absorber highly depend on its electromagnetic parameters, i.e., the complex permittivity (ε_r) and complex permeability (μ_r). To confirm the relative complex permittivity and permeability, the paraffin wax based CF/$Co_{0.2}Fe_{2.8}O_4$/PANI composite was fabricated via compressing. As shown in Fig. 5, the complex permittivity ($\varepsilon_r=\varepsilon'-j\varepsilon''$) and complex permeability ($\mu_r=\mu'-j\mu''$) of the CF/$Co_{0.2}Fe_{2.8}O_4$/PANI wax composite

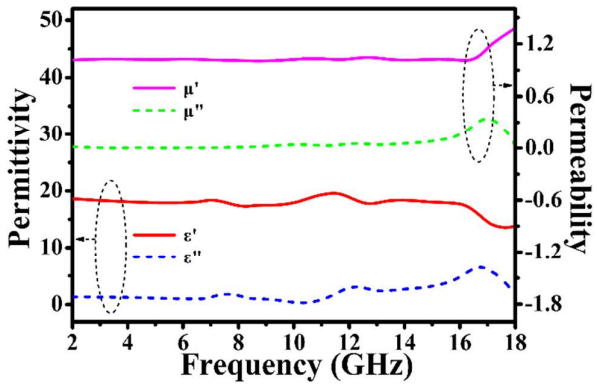

Fig. 5. The real parts and the imaginary parts of the relative permittivity and permeability for CF/$Co_{0.2}Fe_{2.8}O_4$/PANI.

were observed in the EM wave frequency range 2−18 GHz.

As shown in Fig. 5, besides slight peaks found at about 7.2 and 11.2 GHz, the real part of the permittivity (ε′) was found to decrease with increasing frequency in the investigated region. To the best of our knowledge, some carbon materials, for instance, graphene, carbon nanotubes, carbon fibers, and carbon nanocoils, commonly display a frequency dispersion behavior in the EM wave frequency range of 2–18 GHz, that is, their complex permittivity will gradually decrease with the increasing frequency. [38] Moreover, the above frequency dispersion behavior can still exist in many carbon material based composites with different magnetic components. Thus, in our case, the wax based CF/$Co_{0.2}Fe_{2.8}O_4$/PANI composite has a similar frequency dispersion behavior in ε′ value. However, it is very interesting that the imaginary part values (ε″) of the composite shows a distinguishable frequency-dependence behavior with an increasing tendency especially in the frequency 10-18 GHz. It is well known that the real parts and the imaginary parts of the relative complex permittivity represent the storage and loss of electric energy. From the above, accordingly, it is evident that the synthesized material CF/$Co_{0.2}Fe_{2.8}O_4$/PANI has obvious dielectric loss properties, i.e., better energy storage and fine EM wave energy dissipation capability. Because the partially amorphous nature of CF as detected by XRD shown in Fig. 1 will lead to many defects on the surface of CF, which can serve as effective polarization centers when exposed beneath the microwave irradiation. [39] Additionally, interfacial polarization and associated relaxation will happen between CF and the coatings ($Co_{0.2}Fe_{2.8}O_4$ layer and PANI layer) for the plentiful interfaces of the three-phase heterostructures composite. Consequently，with the strong cooperation of different polarization models and relaxation process mentioned above, plenty of charges can accumulate at the interfaces, which finally result in the special dielectric performance of CF/$Co_{0.2}Fe_{2.8}O_4$/PANI. [38, 40] In brief, all of these results together indicate that the CF based LBL structure plays a significant role in determining the dielectric loss properties of the three-phase heterostructure absorber.

However, as shown in Fig. 5, there is a normal resonance phenomenon between μ′ and μ″. For μ′, the value is around 1.02 and display week peaks with the increasing of EM wave frequency in the frequency range of 5-16 GHz, and then gradually increase to 1.33 at 18 GHz. The μ″ curve has a similar behavior with weak peaks in 5-15 GHz and the highest fluctuations at around 17 GHz. These high resonance frequencies are mainly attributed to the small size effect and confinement effect. [34, 41, 42] As discussed above, the complex permeability of CF/$Co_{0.2}Fe_{2.8}O_4$/PANI was dominated by the coated $Co_{0.2}Fe_{2.8}O_4$ nanoparticles on the surface of CF. Moreover, CF/$Co_{0.2}Fe_{2.8}O_4$/PANI also inherited the normal resonance phenomenon and magnetic loss ability of $Co_{0.2}Fe_{2.8}O_4$ nanoparticles at the same time. It is believable that the magnetic loss from the $Co_{0.2}Fe_{2.8}O_4$ magnetic nanoparticles and the dielectric loss caused by CF, PANI and the special structure will finally contribute to enhancement in the reflection loss (RL) for a better performance of EM wave absorbency.

Microwave absorption properties

When EM wave is incident on the surface of the absorber, part of the wave energy is reflected on the surface and the wave inside the absorber is attenuated. The reflection on the surface is determined by the input characteristic impedance (Z_{in}) and the characteristic impedance of free space (Z_0): [27]

$$\Gamma = (Z_{in}-Z_0)/(Z_{in}+Z_0) \quad (1)$$

Moreover, the EM wave attenuation ability inside the absorber is related to the attenuation constant α expressed as: [30]

$$\alpha = \frac{\pi f}{c}\sqrt{2\mu'\varepsilon'}\sqrt{\frac{\mu''\varepsilon''}{\mu'\varepsilon'}-1+\sqrt{\left(\frac{\mu''}{\mu'}\right)^2+\left(\frac{\varepsilon''}{\varepsilon'}\right)^2+\left(\frac{\mu''\varepsilon''}{\mu'\varepsilon'}\right)^2+1}} \quad (2)$$

Undoubtedly, as mentioned above, both the reflection factor (Γ) and the attenuation constant (α) are function of the electromagnetic parameters. Furthermore, the real parts and the imaginary parts of the relative complex permittivity and the relative complex permeability represent the storage and loss of EM wave energy. Accordingly, the EM wave absorbency of absorber can be determined by the obtained electromagnetic parameters. On the basis of the obtained electromagnetic parameter of the absorber stretched in Fig. 5, the EM wave reflection loss property (RL, in dB unit) of CF/$Co_{0.2}Fe_{2.8}O_4$/PANI was investigated based on the transmission line theory evaluated by the following equations:

$$Z_0 = \sqrt{\mu_0/\varepsilon_0} \quad (3)$$

$$Z_{in} = Z_0\sqrt{\mu_r/\varepsilon_r}\tanh[j(2\pi fd/c)\sqrt{\mu_r\varepsilon_r}] \quad (4)$$

$$RL=20\lg\left|(Z_{in}-Z_0)/(Z_{in}+Z_0)\right| \quad (5)$$

where Z_0 is the characteristic impedance of free space (air), μ_0 and ε_0 are the complex relative permeability and permittivity of free space, while Z_{in} is the input characteristic impedance of the absorber, f is the EM wave frequency, d is the thickness of the absorber material, c is the velocity of electromagnetic waves in free space (3×10^8 m/s). ε_r and μ_r are the complex permittivity ($\varepsilon_r=\varepsilon'-j\varepsilon''$) and permeability ($\mu_r=\mu'-j\mu''$) of the absorber, respectively. [38, 43] The simulated reflection loss-frequency (RL-F) curves are illustrated in Fig. 6, and it is found to be sensitive to the absorber sample thickness.

Shown in Fig. 6, with increasing in the absorber sample thickness,

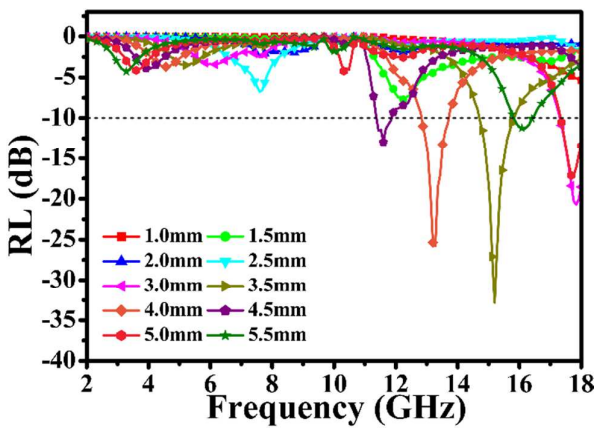

Fig. 6. The relationship between RL-F for CF/$Co_{0.2}Fe_{2.8}O_4$/PANI in 2-18 GHz range with the thickness from 1.0 to 5.5 mm.

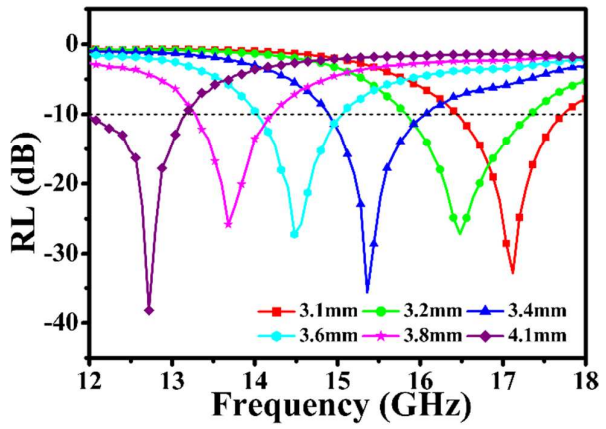

Fig. 7. The relationship between RL-F for CF/$Co_{0.2}Fe_{2.8}O_4$/PANI in K_u band (12-18 GHz) with the thickness from 3.1 to 4.1 mm.

the strong peak position has a tendency toward lower frequency range. According to the quarter-wavelength cancellation model, it is known that the minimal reflections can be achieved at a certain EM range. According to the quarter-wavelength cancellation model, it is known that the minimal reflections can be achieved at a certain EM wave frequency if the thickness of the absorber composite satisfies the matching equation:[12]

$$d = nc/(4f\sqrt{|\varepsilon_r||\mu_r|}) \quad (n=1, 3, 5\ldots) \qquad (6)$$

Consequently, the attenuation peaks shift to the lower frequency regions and more attenuation peaks might appear as the thickness of the absorbers increases. Obviously, the RL value of the three-phase heterostructure CF/$Co_{0.2}Fe_{2.8}O_4$/PANI composites below -10 dB, which means that 90% of the incident EM wave energy is absorbed, can be achieved in the 11–18 GHz range with the thickness of 3.0–5.0 mm. Moreover, the minimum RL value of -32.8 dB can be gained at 15.2 GHz with a matching thickness of 3.5 mm. For comparison, the simulated reflection loss-frequency (RL-F) curves of CF/$Co_{0.2}Fe_{2.8}O_4$ are illustrated in Fig. S3. For CF/$Co_{0.2}Fe_{2.8}O_4$, with the thickness 4.0-5.5 mm, the RL value below -10 dB can be obtained in the EM frequency range 11-18 GHz. However, the minimum RL value of the absorption curves are all around -20 dB, which is bigger than that of CF/$Co_{0.2}Fe_{2.8}O_4$/PANI. And the matching thickness of CF/$Co_{0.2}Fe_{2.8}O_4$ is higher than that of CF/$Co_{0.2}Fe_{2.8}O_4$/PANI. From the above results, it was confirmed that CF/$Co_{0.2}Fe_{2.8}O_4$/PANI has a better EM wave absorbency ability, especially in the EM wave K_u band. To further verify the results, the EM wave reflection loss ability was also checked in the K_u band 12-18 GHz with the absorber thickness of 3.1-4.1 mm. As sketched in Fig. 7, it is evident that the minimum RL values are all lower than -20 dB, which means more than 99 % of the incident EM wave energy can be attenuated. [12] Furthermore, with a thickness of 4.1 mm, the minimum RL value of -38.2 dB can be achieved at 12.7 GHz. Compared to the EM wave attenuation ability of recent CF based EM wave absorber as presented in Table 1, the three-phase LBL heterostructure absorber CF/$Co_{0.2}Fe_{2.8}O_4$/PANI has a relatively strong EM wave absorbency. To conclude, the synthesized three-phase heterostructure absorber CF/$Co_{0.2}Fe_{2.8}O_4$/PANI has an excellent EM wave absorbency in the EM wave K_u band.

Table 1 EM wave absorption performance of representative CF-based absorbers.

Absorber	wt%	Max RL (dB)	RL<-10 dB
BN/SiC/CF[44]	20%	-13.3	11-13.5
CF and CI[45]	2 % CF 65% CI	-14	8-18
Carbon coil-CF[33]	10%	-17.3	7.8-16.2
Double-carbon microcoils-CFs[46]	10%	20.2	11.1-15.6
Hollow CF[47]	33.3% (V)	-21.4	9-12
CuO/CF[48]	60%	-29.6	2.7-15.9
MCCFs-2[49]	50%	-30	2-12
Fe_3O_4/CFs[50]	50%	-35	4-10
CF/$Co_{0.2}Fe_{2.8}O_4$/PANI (this work)	33%	-38.2	12-18

For an excellent absorber, there are two key factors that should be taken into consideration. One is the impedance matching condition, which allows EM wave to propagate into the absorber sufficiently and avoids the strong reflection, this is also the precondition of EM wave absorption. [51] It is well known than in an optimal situation, the EM matching is illustrated by the equation: $\mu''=\varepsilon''$ and $\mu'=\varepsilon'$. However, the permittivity and permeability can't meet the above equation in different frequencies in the same medium because both of permittivity and permeability are function of frequency. Also, for most synthesized composite materials, the permittivity is usually higher than permeability. Under this circumstance, a generalized EM matching equation is used as a criterion to effectively choice EM wave absorption materials: $\mu'/\varepsilon'=\mu''/\varepsilon''$. Thus, a defined δ can be used to evaluate the coefficient EM matching condition using the equation: $\delta=(\mu''/\varepsilon'')/(\mu'/\varepsilon')$. [4] The EM matching performs much better with δ value close to one. The δ of the synthesized two-phase absorber CF/$Co_{0.2}Fe_{2.8}O_4$ and three-phase absorber CF/$Co_{0.2}Fe_{2.8}O_4$/PANI are plotted as a function of frequency in Fig. S4. In K_u band, the δ value of CF/$Co_{0.2}Fe_{2.8}O_4$ and CF/$Co_{0.2}Fe_{2.8}O_4$/PANI are all close to 1. Though an optimal matching condition is not achieved, the matching conditions of the synthesized two-phase and three-phase absorbers are relatively fine. In this work, PANI layer and $Co_{0.2}Fe_{2.8}O_4$ layer with the relatively low conductivity were as the coating outside CF. Apparently, the higher impedance values would lead to lower reflection effectiveness. [52] Thus, EM wave can propagate into the absorber to be attenuated rather than reflected on the absorber surface. Hence, the PANI layer and $Co_{0.2}Fe_{2.8}O_4$ layer play an important role in determining the EM wave absorption characteristic of the three-phase heterostructures absorber. The other key factor is the best EM wave attenuation performance inside the absorber. An excellent absorber can attenuate the incident EM wave rapidly through the absorber layer, and reduce the emerging wave to an acceptable low magnitude. [51] It is well known that when an EM wave is incident on the absorber sample, there are two possible contributions for the EM wave absorption, that is, dielectric loss and magnetic loss. [23] And a higher value of loss tangent indicates a higher EM wave loss. For a better understanding of the EM wave attenuation ability

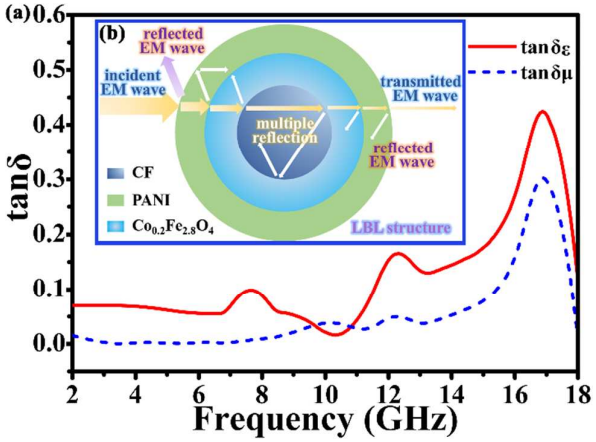

Fig. 8. (a) Frequency dependence of the loss tangent for CF/$Co_{0.2}Fe_{2.8}O_4$/PANI in 2-18 GHz; (b) EM wave spread schemes of CF/$Co_{0.2}Fe_{2.8}O_4$/PANI.

of CF/$Co_{0.2}Fe_{2.8}O_4$/PANI, Fig. 8a shows the calculated dielectric loss tangent ($\tan\delta_\varepsilon=\varepsilon''/\varepsilon'$) and magnetic loss tangent ($\tan\delta_\mu=\mu''/\mu'$). In the EM wave frequency range 2-18 GHz, the dielectric loss tangent is higher than magnetic loss tangent with an exception at 10-11 GHz, suggesting a better dielectric loss ability of CF/$Co_{0.2}Fe_{2.8}O_4$/PANI than magnetic loss ability. [15] However, different from the low values of $\tan\delta_\varepsilon$ and $\tan\delta_\mu$ in 2-11 GHz, both $\tan\delta_\varepsilon$ and $\tan\delta_\mu$ keep in relatively high values in 12-18 GHz. For comparison, the $\tan\delta_\varepsilon$ and $\tan\delta_\mu$ of CF/$Co_{0.2}Fe_{2.8}O_4$ are stretched in Fig. S5a. The value of $\tan\delta_\varepsilon$ and $\tan\delta_\mu$ are all under 0.1 with some fluctuations which are lower than that of CF/$Co_{0.2}Fe_{2.8}O_4$/PANI. It is clear that the values of loss tangent for CF/$Co_{0.2}Fe_{2.8}O_4$/PANI are obviously enhanced after coating with a layer of PANI. Moreover, in our study, for CF/$Co_{0.2}Fe_{2.8}O_4$/PANI, the LBL structure effectively increased the propagation of EM wave in the course of its interior as shown in Fig. 8b. Compared to the two-phase heterostructure absorber CF/$Co_{0.2}Fe_{2.8}O_4$ shown in Fig. S5b, by multiple reflections between the layer and layer interfaces, the interaction of CF/$Co_{0.2}Fe_{2.8}O_4$/PANI absorber and EM wave is strongly enhanced. The results further confirm the better EM wave attenuation ability of CF/$Co_{0.2}Fe_{2.8}O_4$/PANI in K_u band. Consequently, considering the combination of dielectric loss and magnetic loss inside the absorber shown in Fig. 8a, the EM wave attenuation ability is effectively improved. [30] Though the matching condition of CF/$Co_{0.2}Fe_{2.8}O_4$ is better than that of CF/$Co_{0.2}Fe_{2.8}O_4$/PANI obtained from the δ value, the loss ability inside the absorber is also important because it can help to rapidly attenuate the incident EM wave energy. Thus, in this work, the three-phase LBL heterostructure composite CF/$Co_{0.2}Fe_{2.8}O_4$/PANI has the better EM wave absorbency.

Ultimately, as mentioned above, CF/$Co_{0.2}Fe_{2.8}O_4$/PANI has a better EM wave absorption ability than that of CF/$Co_{0.2}Fe_{2.8}O_4$ for three major reasons. Firstly, a PANI layer can serve as an effective coating to prevent $Co_{0.2}Fe_{2.8}O_4$ nanoparticles from oxidation, which will further enhance the stability of $Co_{0.2}Fe_{2.8}O_4$ in the three-phase heterostructures absorber for a fine magnetic loss ability. [53] Secondly, the low conductivity of PANI can contribute to the propagation of EM wave in the absorber by reducing the reflection on the absorber surface. Lastly, the introduction of PANI coating layer may help to improve the interfaces and the interaction between the absorber and EM wave, which will finally results in a better EM wave loss performance. Moreover, it is reported that the PANI coating layer outside CF/$Co_{0.2}Fe_{2.8}O_4$/PANI can also improve the compatibility between absorber and matrix. [15] As already suggested by the results, it is evident that CF/$Co_{0.2}Fe_{2.8}O_4$/PANI, superior to CF/$Co_{0.2}Fe_{2.8}O_4$, are excellent fillers for enhanced microwave absorption based on both improved dielectric and magnetic properties. The EM attenuation property of CF is thus enhanced. Therefore, it is a significant role in designing and fabrication of high performance EM wave absorption materials by introducing some specially designed multiple phase.

Conclusions

A three-phase heterostructures composite CF/$Co_{0.2}Fe_{2.8}O_4$/PANI has been successfully synthesized to improve the EM wave absorbency of CF and the structure and morphology have been investigated in detail. It is evident that the LBL heterostructures of CF/$Co_{0.2}Fe_{2.8}O_4$/PANI contributes to a better performance of EM wave attenuation. CF/$Co_{0.2}Fe_{2.8}O_4$/PANI has a strong EM wave attenuation ability in EM wave K_u band. With a thickness of 4.1 mm, an optimal RL of -38.2 dB (>99.9 % attenuation) is observed at 12.7 GHz. Moreover, with the thickness from 3.1 to 4.1 mm, the minimum RL curves in K_u band are all lower than -20 dB. The enhanced EM absorption ability results from the combined effect of magnetic loss and dielectric loss and the fine EM matching condition simultaneously. By introducing more specially designed phase onto CF, the EM wave absorption property was strongly enhanced. The three-phase heterostructures composite CF/$Co_{0.2}Fe_{2.8}O_4$/PANI can be a potential material for application in EM wave absorption field. And the approach to improve the EM wave absorbency of CF in this study also provides new opportunities for designing other EM wave attenuation materials.

Acknowledgements

This work was financially supported by the National Science Foundation (51003038). Also the authors express their great thanks for the kindly help of M.S. Yue Zhao from the State Key Laboratory of Inorganic Synthesis and Preparative Chemistry and Prof. Lifeng Wang from Alan G. MacDiarmid Institute in structural characterization.

References

1 F. Wu, Y. Wang and M. Y. Wang, *RSC Adv.*, 2014, **4**, 49780-49782.
2 R. Kumar, A. P. Singh, M. Chand, R. P. Pant, R. K. Kotnala, S. K. Dhawan, R. B. Mathur and S. R. Dhakate, *RSC Adv.*, 2014, **4**, 23476-23484.
3 Z. H. Yang, Z. W. Li, L. H. Yu, Y. H. Yang and Z. C. Xu, *J. Mater. Chem. C*, 2014, **2**, 7583-7588.
4 Z. Zhonglun, J. Zhijiang, D. Yuping, G. Shuchao and G. Jingbo, *Journal of Materials Science: Materials in Electronics*, 2013, **24**, 968-973.
5 Y. Wang, L. Wang and H. Wu, *Materials* 2013, **6**, 1520-1529.

6 D. P. Sun, Q. Zou, Y. P. Wang, Y. J. Wang, W. Jiang and F. S. Li, *Nanoscale*, 2014, **6**, 6557-6562.
7 X. H. Li, J. Feng, H. Zhu, C. H. Qu, J. T. Bai and X. L. Zheng, *RSC Adv.*, 2014, **4**, 33619-33625.
8 Y. L. Ren, C. L. Zhu, L. H. Qi, H. Gao and Y. J. Chen, *RSC Adv.*, 2014, **4**, 21510-21516.
9 X. B. Li, S. W. Yang, J. Sun, P. He, X. P. Pu and G. Q. Ding, *Synthetic. Met.*, 2014, **194**, 52-58.
10 G. Shen, M. Xu and Z. Xu, *Mater. Chem. Phys.*, 2007, **105**, 268-272.
11 H. Wu, L. Wang, Y. Wang and S. Guo, *Appl. Surf. Sci.*, 2012, **258**, 10047-10052.
12 J. Xiang, J. L. Li, X. H. Zhang, Q. Ye, J. H. Xu and X. Q. Shen, *J. Mater. Chem. A*, 2014, **2**, 16905-16914.
13 G. L. Wu, Y. H. Cheng, Q. Xie, Z. R. Jia, F. Xiang and H. J. Wu, *Mater. Lett.*, 2015, **144**, 157-160.
14 H. Wu, L. Wang, Y. Wang, S. Guo and Z. Shen, *Materials Science and Engineering: B*, 2012, **177**, 476-482.
15 M. S. Cao, J. Yang, W. L. Song, D. Q. Zhang, B. Wen, H. B. Jin, Z. L. Hou and J. Yuan, *Acs Appl. Mater. Interfaces*, 2012, **4**, 6948-6955.
16 S. Varshney, A. Ohlan, V. K. Jain, V. P. Dutta and S. K. Dhawan, *Ind. Eng. Chem. Res.*, 2014, **53**, 14282-14290.
17 Z. F. He, Y. Fang, X. J. Wang and H. Pang, *Synthetic. Met.*, 2011, **161**, 420-425.
18 Q. L. Liu, J. J. Gu, W. Zhang, Y. Miyamoto, Z. X. Chen and D. Zhang, *J. Mater. Chem.*, 2012, **22**, 21183-21188.
19 H. S. Wang, G. B. Wang, W. L. Li, Q. T. Wang, W. Wei, Z. H. Jiang and S. L. Zhang, *J. Mater. Chem.*, 2012, **22**, 21232-21237.
20 S. P. Pawar, D. A. Marathe, K. Pattabhi and S. Bose, *J. Mater. Chem. A*, 2015, **3**, 656-669.
21 Z. T. Zhu, X. Sun, H. R. Xue, H. Guo, X. L. Fan, X. C. Pan and J. P. He, *J. Mater. Chem. C*, 2014, **2**, 6582-6591.
22 X. Jian, X. N. Chen, Z. W. Zhou, G. Li, M. Jiang, X. L. Xu, J. Lu, Q. M. Li, Y. Wang, J. H. Gou and D. Hui, *Phys. Chem. Chem. Phys.*, 2015, **17**, 3024-3031.
23 C. Feng, X. G. Liu, Y. P. Sun, C. G. Jin and Y. H. Lv, *RSC Adv.*, 2014, **4**, 22710-22715.
24 J. J. Jiang, D. Li, S. J. Li, Z. H. Wang, Y. Wang, J. He, W. Liu and Z. D. Zhang, *RSC Adv.*, 2015, **5**, 14584-14591.
25 B. A. Zhao, G. Shao, B. B. Fan, W. Y. Zhao, Y. Q. Chen and R. Zhang, *RSC Adv.*, 2015, **5**, 9806-9814.
26 H. Wang, H. Guo, Y. Dai, D. Geng, Z. Han, D. Li, T. Yang, S. Ma, W. Liu and Z. Zhang, *Appl. Phys. Lett.*, 2012, **101**, 083116.
27 F. Qin and C. Brosseau, *J. Appl. Phys.*, 2012, **111**, 061301.
28 H. Wu, L. Wang and H. Wu, *Appl. Surf. Sci.*, 2014, **290**, 388-397.
29 L. Wang, H. Wu, Z. Shen, S. Guo and Y. Wang, *Materials Science and Engineering: B*, 2012, **177**, 1649-1654.
30 L. Yuan, L. Xiangxuan, L. Rong, W. Wu and W. Xuanjun, *RSC Adv.*, 2015, **5**, 8713-8720.
31 B.-F. Zhao, P. Ma, J.-M. Zhao, D.-A. Li and X. Yang, *Ceram. Int.*, 2013, **39**, 2317-2322.
32 H. Luo, G. Xiong, Z. Yang, Q. Li, C. Ma, D. Li, R. Guo and Y. Wan, *Surf Coat Technol*, 2014, **253**, 180-184.
33 L. Liu, K. Zhou, P. He and T. Chen, *Mater. Lett.*, 2013, **110**, 76-79.
34 W. Wei, X. Yue, Y. Zhou, Z. Chen, J. Fang, C. Gao and Z. Jiang, *Phys. Chem. Chem. Phys.*, 2013, **15**, 21043-21050.
35 P. Liu, Y. Huang and X. Zhang, *J. Alloy. Compd.*, 2014, **596**, 25-31.
36 J. Zou, Q. Liu, Z. Zi and J. Dai, *Mater. Res. Innov.*, 2014, **18**, 304-309.
37 H. Xia, B. Cui, J. Zhou, L. Zhang, J. Zhang, X. Guo and H. Guo, *Appl. Surf. Sci.*, 2011, **257**, 9397-9402.
38 Y. C. Du, W. W. Liu, R. Qiang, Y. Wang, X. J. Han, J. Ma and P. Xu, *Acs Appl. Mater. Interfaces*, 2014, **6**, 12997-13006.
39 L. Pisani, B. Montanari and N. M. Harrison, *New J. Phys.*, 2008, **10**, 033002.
40 Y.-J. Chen, G. Xiao, T.-S. Wang, Q.-Y. Ouyang, L.-H. Qi, Y. Ma, P. Gao, C.-L. Zhu, M.-S. Cao and H.-B. Jin, *J. Phys. Chem. C*, 2011, **115**, 13603-13608.
41 Y.-J. Chen, P. Gao, R.-X. Wang, C.-L. Zhu, L.-J. Wang, M.-S. Cao and H.-B. Jin, *J. Phys. Chem. C*, 2009, **113**, 10061-10064.
42 J. Zhou, J. He, G. Li, T. Wang, D. Sun, X. Ding, J. Zhao and S. Wu, *J. Phys. Chem. C*, 2010, **114**, 7611-7617.
43 G. Liu, L. Y. Wang, G. M. Chen, S. C. Hua, C. Q. Ge, H. Zhang and R. B. Wu, *J. Alloy. Compd.*, 2012, **514**, 183-188.
44 X. P. ZHOU Wei, LI Yang, LUO Heng, HONG Wen, *J. Inorg. Mater.*, 2014, **29**, 1093-1098.
45 Y. C. Qing, W. C. Zhou, S. Jia, F. Luo and D. M. Zhu, *Appl Phys A*, 2010, **100**, 1177-1181.
46 L. Liu, P. He, K. Zhou and T. Chen, *J. Mater. Sci.*, 2014, **49**, 4379-4386.
47 W. Xie, H. Cheng, Z. Chu and Z. Chen, *J. Inorg. Mater.*, 2008, **23**, 481-485.
48 J. Zeng, J. Xu, P. Tao and W. Hua, *J. Alloy. Compd.*, 2009, **487**, 304-308.
49 X. Meng, Y. Wan, Q. Li, J. Wang and H. Luo, *Appl. Surf. Sci.*, 2011, **257**, 10808-10814.
50 C. Qiang, J. Xu, Z. Zhang, L. Tian, S. Xiao, Y. Liu and P. Xu, *J. Alloy. Compd.*, 2010, **506**, 93-97.
51 X. Meng, Y. Wan, Q. Li, J. Wang and H. Luo, *Appl. Surf. Sci.*, 2011, **257** 10808-10814.
52 W. L. Song, M. S. Cao, L. Z. Fan, M. M. Lu, Y. Li, C. Y. Wang and H. F. Ju, *Carbon*, 2014, **77**, 130-142.
53 Z. Liu, J. Wang, D. Xie and G. Chen, *Small*, 2008, **4**, 462-466.